NUMERICAL INVESTIGATION OF INCOMPRESSIBLE FLUID FLOW AND HEAT TRANSFER ACROSS A BLUFF BODY IN A CHANNEL FLOW

by

Imdat TAYMAZ [a]*, Erman ASLAN [a], and Ali Cemal BENIM [b]

[a] Department of Mechanical Engineering, University of Sakarya, Adapazari, Turkey
[b] Department of Mechanical Engineering and Process Engineering, Dusseldorf University of Applied Sciences, Dusseldorf, Germany

Original scientific paper
DOI: 10.2298/TSCI120220145T

The lattice Boltzmann method is applied to computationally investigate the laminar flow and heat transfer of an incompressible fluid with constant material properties in a 2-D channel with a built-in bluff body. In this study, a triangular prism is taken as the bluff body. Not only the momentum transport, but also the energy transport is modeled by the lattice Boltzmann method. A uniform lattice structure with a single time relaxation rule is used. For obtaining a higher flexibility on the computational grid, interpolation methods are applied, where the information is transferred from the lattice structure to the computational grid by Lagrange interpolation. The flow is investigated for different Reynolds numbers, while keeping the Prandtl number at the constant value of 0.7. The results show how the presence of a triangular prism effects the flow and heat transfer patterns for the steady-state and unsteady-periodic flow regimes. As an assessment of the accuracy of the developed lattice Boltzmann code, the results are compared with those obtained by a commercial computational fluid dynamics code. It is observed that the present lattice Boltzmann code delivers results that are of similar accuracy to the well-established computational fluid dynamics code, with much smaller computational time for the prediction of the unsteady phenomena.

Key words: *lattice Boltzmann method, channel flow with bluff body, interpolation supplemented lattice Boltzmann method*

Introduction

Flow around bluff bodies in ducts and channels has been investigated intensively by many researchers, both experimentally [1-3] and numerically [4-6], since this flow is of importance for different applications including electronic cooling and heat exchange systems. Within this context, a triangular prism as a bluff body is a basic configuration. Abbasi *et al*. [7] analysed the incompressible laminar flow and heat transfer in a 2-D channel with a built-in triangular prism computationally. They showed that the use a triangular prism could enhance the heat transfer to the channel walls. Chattopadhyay [8] investigated a similar configuration numerically for incompressible turbulent flows, by applying a steady-state Reynolds averaged Navier-Stokes equations (RANS) analysis based on a two-equation turbulence model. The pre-

* Corresponding author; e-mail: taymaz@sakarya.edu.tr

vious computational work [4-8] was principally based on the discretization of the Navier-Stokes equations. Also, Ellahi [9] is explained basics, concepts and methods of steady and unsteady flow for Newtonian and non-Newtonian fluids. Additionally, effects of the Reynolds and Prandtl numbers on incompressible fluids and heat transfer can be found in [9]. The novelty of the present investigation is the application of the lattice Boltzmann method (LBM) [10, 11] to analyze the problem. The presently developed 2-D LBM code for incompressible flows, which was recently applied [12] to several benchmark isothermal, steady-state flow problems is extended, in the present work, to include the transport of thermal energy. This code is now used to analyze the laminar fluid flow and heat transfer in a plane channel, with a built-in triangular prism, which also exhibits an unsteady-periodic nature due to the vortex shedding behind the prism, depending on the Reynolds number. Results are compared with those obtained by a commercial computational fluid dynamics (CFD) code Fluent [13]. In these comparisons, both accuracy, and computational costs of LBM against conventional CFD procedures are assessed. Recently, a similar problem, namely, the forced convection in a plane-channel with built-in square obstacles was investigated by LBM by Moussaoui *et al*. [14]. However, in that work, the flow was modeled by LBM, whereas the energy equation was discretized by the finite difference method. In difference to the previous work [10], the temperature distribution is also computed by LBM, in the present analysis.

In comparison to the previous work of the present authors [12], for obtaining a higher flexibility on the computational grid, the present LBM code has been further developed to incorporate interpolation methods [15-20], where the information is transferred from the lattice structure to the computational grid by Lagrange interpolation.

Problem definition

The investigated geometry is similar to the one, which was computationally investigated by Abbasi *et al*. [7] using a control volume based finite element method. The geometry is shown in fig. 1.

In fig. 1, the half of the solution domain is shown, which is enclosed by a symmetry boundary at the channel mid-height, running through the middle of the triangular prism (TP). Although the time-averaged flow needs to be symmetric around this plane, the time dependent flow is not, of course, for higher Reynolds numbers, where the flow becomes unsteady, and exhibits vortex shedding behind the prism. A steady-state solution can, however, still be enforced, by using an artificial symmetry plane as shown in fig. 1. In the present computations, irrespective of the Reynolds number, a steady-state solution is also obtained by using this symmetry plane, for comparison purposes (as such simplification are sometimes being done, for some flows, for practical purposes, assuming that the steady-state solution obtained this way would resemble the time-averaged solution). For the main, unsteady computations, the domain is twice as large as the one shown, mirrored around the symmetry plane (fig. 1) and, thus, exhibiting no symmetry plane through the middle of the channel, of course.

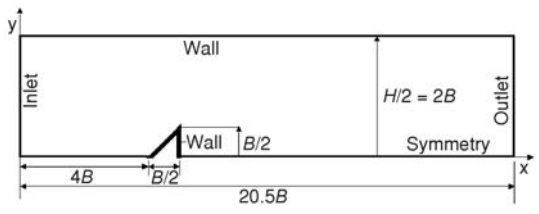

Figure 1. Half of the domain, boundary types

For the momentum equations, a parabolic, fully developed channel flow velocity profile is imposed as boundary condition at the inlet, and a constant static pressure is prescribed at the outlet. No-slip boundary conditions apply at the walls. For the energy equation a constant temperature is pre-

scribed at the inlet boundary. Adiabatic prism walls are assumed, while zero-gradient boundary conditions is applied at the outlet. Channel walls, are prescribed to be isothermal.

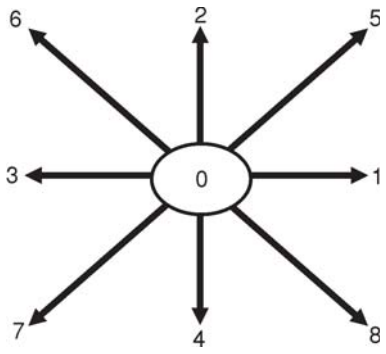

Figure 2. D2Q9 lattice model

LBM formulation

Mostly used LBM formulations are based on the single relaxation time approximation of Bhatnagar-Gross-Krook (BGK) [21]. In the present work, a version due to He and Luo [22] is adopted, which is especially suitable for unsteady, incompressible flows. The 2-D 9-velocity lattice model (D2Q9) is used, which is displayed in fig. 2.

According to the present modeling, using two different distribution functions, one for the density (momentum) and one for the temperature, the discretized lattice Boltzmann evolution equations for momentum and energy transport, which are usually solved in two consecutive steps, *i. e*. in a "collision" and a following "streaming" step, are:

– collision

$$\tilde{f}_\alpha(\vec{\mathrm{x}}, t+\delta t) = f_\alpha(\vec{\mathrm{x}}, t) - \omega[f_\alpha(\vec{\mathrm{x}}, t) - f_\alpha^{eq}(\vec{\mathrm{x}}, t)] \tag{1a}$$

$$\tilde{g}_\alpha(\vec{\mathrm{x}}, t+\delta t) = g_\alpha(\vec{\mathrm{x}}, t) - \omega_T[g_\alpha(\vec{\mathrm{x}}, t) - g_\alpha^{eq}(\vec{\mathrm{x}}, t)] \tag{1b}$$

– streaming

$$f_\alpha(\vec{\mathrm{x}} + \vec{\mathrm{e}}_\alpha \delta t,\ t+\delta t) = \tilde{f}_\alpha(\vec{\mathrm{x}}, t+\delta t) \tag{2a}$$

$$g_\alpha(\vec{\mathrm{x}} + \vec{\mathrm{e}}_\alpha \delta t,\ t+\delta t) = \tilde{g}_\alpha(\vec{\mathrm{x}}, t+\delta t) \tag{2b}$$

The collision frequencies are defined by:

$$\omega = \frac{1}{\dfrac{\nu}{c_s^2 \delta t} + \dfrac{1}{2}} \tag{3a}$$

$$\omega_{\mathrm{T}} = \frac{1}{\dfrac{a}{c_s^2 \delta t} + \dfrac{1}{2}} \tag{3b}$$

where the lattice sound speed c_{s} and lattice speed c are defined as:

$$c_{\mathrm{s}} = \frac{c}{\sqrt{3}} \tag{4}$$

$$c = \frac{\delta}{\delta t} \tag{5}$$

The nine discrete velocities of the model are:

$$\vec{\mathrm{e}}_\alpha = c\begin{bmatrix} 0 & 1 & 0 & -1 & 0 & 1 & -1 & -1 & 1 \\ 0 & 0 & 1 & 0 & -1 & 1 & 1 & -1 & -1 \end{bmatrix} \tag{6}$$

The equilibrium distribution functions are:

$$f_\alpha^{eq} = w_\alpha \left\{ \rho + \rho_0 \left[\frac{3}{c^2} \vec{\mathrm{e}}_\alpha \vec{\mathrm{u}} + \frac{9}{2c^4} (\vec{\mathrm{e}}_\alpha \vec{\mathrm{u}})^2 - \frac{3}{2c^2} \vec{\mathrm{u}}\vec{\mathrm{u}} \right] \right\} \tag{7a}$$

$$g_\alpha^{eq} = w_\alpha T\left[1 + \frac{3}{c^2}\vec{e}_\alpha \vec{u}\right] \tag{7b}$$

with

$$w_\alpha = \left[\frac{4}{9} \quad \frac{1}{9} \quad \frac{1}{9} \quad \frac{1}{9} \quad \frac{1}{9} \quad \frac{1}{36} \quad \frac{1}{36} \quad \frac{1}{36} \quad \frac{1}{36}\frac{1}{36}\right] \tag{8}$$

The macroscopic fields are obtained from:

$$p_\alpha = c_s^2 f_\alpha \tag{9a}$$

$$p_\alpha^{eq} = c_s^2 f_\alpha^{eq} \tag{9b}$$

$$p = \sum_{\alpha=0}^{8} p_\alpha = \sum_{\alpha=0}^{8} p_\alpha^{eq} \tag{9c}$$

$$\vec{u} = \frac{1}{p_0}\sum_{\alpha=0}^{8}\vec{e}_\alpha p_\alpha = \frac{1}{p_0}\sum_{\alpha=0}^{8}\vec{e}_\alpha p_\alpha^{eq} \tag{10}$$

$$T = \sum_{\alpha=0}^{8} g_\alpha = \sum_{\alpha=0}^{8} g_\alpha^{eq} \tag{11}$$

The time step size δt is chosen in such a way to result in a lattice speed c (5) of unity, resulting in a lattice sound speed s_c (4) of magnitude $1/(3)^{1/2}$.

Implementation of boundary conditions are not shown here in detail, for brevity, but can be found, *e. g.* in Succi [11] and Sukop and Daniel [23]. At walls, the so-called "bounce-back" boundary condition is applied for the momentum equations, where the physical boundaries of the solution domain are defined to be aligned with the lattice grid lines ("on-grid" formulation). For coding the model, sample FORTRAN codes provided in Mohammad [10] are used as a basis.

Interpolation supplemented LBM (ISLBM)

In the traditional LBM, a uniform, squarish lattice structure is used in the whole solution domain. The usual CFD practice is, however, to use a variable mesh density, for optimally distributing the nodes between the high and low gradient flow regions. The uniform lattice structure does not allow this, and, thus, leads to an excessively fine overall resolution, and, thus, to a large increase in the operation count and memory requirement. In this context, another problem, which stems from the stability limitations of the standard LBM, is that the lattice spacing needs to be finer with increasing Reynolds number, leading to excessively fine lattice structures for high Reynolds number, and, thus, again to high computational costs. For better coping with these limitations, several methods, including the so-called Interpolation Supplemented LBM (ISLBM) [15-20] were proposed.

In ISLBM, a non-uniform (finite difference like) computational grid is used, which allows the nodes to be distributed according to the needs of the problem. The nodes of this grid do not need to coincide with the underlying lattice structure. The distribution functions are evaluated and stored only at the nodes of the computational grid. Collision takes place at the nodes of the computational grid. However, the streaming step results in the values of the distribution function being available off-grid. Thus, the distribution functions at the nodes of the computational grid need to be calculated by an appropriate interpolation procedure, *i.e*. Lagrangian interpolation which was first outlined in [15].

In the present work, the ISLBM approach is implemented. The equations for the 2-D Lagrangian interpolation are not presented here, but can be found in [15-20]. Linear interpola-

tion (LI) and second order interpolation schemes are implemented. For the second order interpolation, two schemes are implemented, namely, a central second order scheme (CSOI), and an upwind second order scheme (USOI). For better understanding, the schemes are sketched in fig. 3.

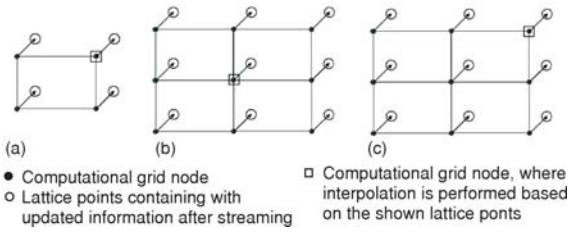

Figure 3. Skecth of the interpolation schemes; (a) LI, (b) CSOI, (c) USOI

In ISLBM, collision takes place at the nodes on computational grid. After that, streaming occurs, but distribution functions can not reach the neighbour computational grid. Therefore, Lagrangian interpolation schemes uses for calculating distribution functions value in computational grid using these unreached distribution functions. As you see in fig. 3, point where interpolation is performed changes, while Lagrange interpolation schemes are changing.

On boundaries, LI can readily be implemented. For the second order interpolation, either CSOI, or USOI is used, depending on the orientation of the boundary and the availability of the nodes.

Results

For validating the present LBM results, the well-established CFD code Fluent [9] is used. An outline of the modeling used in Fluent calculations can be given as follows: A second order upwind procedure is used in discretizing the convective terms. In time, a second-order backward Euler scheme is used. For treating the velocity-pressure coupling, the SIMPLEC scheme is used for steady-state computations, whereas the PISO algorithm is applied for unsteady computations. Default under-relaxation factors are used (pressure: 1.0, momentum: 0.7). As convergence criteria, 100 times smaller tolerances for the scaled residuals are required than the default values (all equations except energy lower than 10^{-5}, the energy equation lower than 10^{-8}).

LBM is an intrinsically unsteady procedure, where, a steady-state solution, if it exists, is found as a result of integration in time. In physically unsteady cases (high enough Reynolds number, without symmetry boundary) always the same time-step size is used for LBM and Fluent calculations. In unsteady computations, the flow starting from any initial distribution is computed for a period of time, until a periodic flow structure gets established. Subsequently, the results are time-averaged for a sufficiently long time for getting time-averaged distributions that are time-invariant.

For a better comparability of the results, always the same computational grids are used for both codes. The only exception is the local grid structure in the vicinity of the triangular prism. In LBM, the triangular shape is approximated by a staircase structure, whereas it is accurately resolved by the finite volume grid of Fluent, using a locally unstructured configuration. For illustration purposes, detail views of the both grids are compared in fig. 4, for a rather coarse resolution, *i. e*. for $N = 4$ (N: number of cells along half base length of the triangular cross-section).

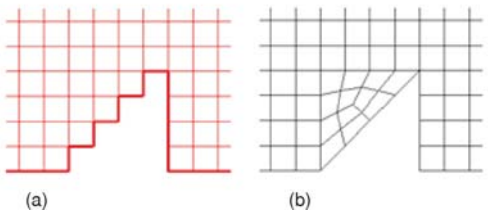

Figure 4. Detail view of grids for $N = 4$; (a) LBM, (b) Fluent

For all computations, Reynolds number is based on density, mean inlet velocity, hydraulic diameter, and dynamic viscosity. For channel flow, hydraulic diameter is taken as two channel height ($2H$).

Preliminary validation

For the implementation of the energy equation (different from [12]), a preliminary validation is performed for laminar forced convection in a fully-developed channel flow. A simple channel geometry (without TP) is modeled for Re = 160, with a constant inlet and a constant wall temperature, with channel length long enough to allow a thermally fully developed flow. The predicted and theoretical [24] Nusselt numbers are compared in tab. 1, where a good agreement is observed.

Table 1. Nu for fully-developed channel flow (Re = 160)

	LBM	Theory [24]
Nu	7.55	7.54

Traditional LBM results

First, the influence of the inaccuracy in representing the shape of TP is investigated. This study is carried out for the steady-state flow, assuming a symmetry boundary through the middle of the prism (fig. 1), for Re = 100. Denoting the number of lattice units/finite volumes along the half-height of the triangular cross-section by N, four different grid resolutions, namely grids with $N = 4$ (fig. 4), 8, 12, and 16 are investigated. Predicted profiles of axial velocity along traversal direction, at an axial position half triangle base behind TP are shown in fig. 5. All predictions are qualitatively similar. Quantitatively, LBM and Fluent predictions for $N = 4$ differ from each other and from the other curves. For $N = 16$, LBM and Fluent predictions perfectly agree with each other. Results for the lower resolutions, *i. e.* for $N = 8$, 12 (not displayed) are very close to those of $N = 16$. In the main computations, a resolution with at least $N = 8$ (or higher) is applied.

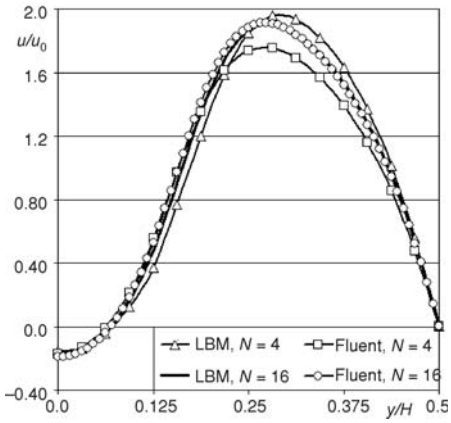

Figure 5. Axial velocity along traversal direction at an axial distance of B/2 downstream for prism (Re = 100)

Table 2 shows the C_D predictions for steady state-flow (symmetry) with four grid resolutions ($N = 4$, 8, 12, 16). For these grid resolutions, used number of total lattice units/finite volumes is given for whole domain in tab. 2. According the table, changes of drag coefficient are so small after $N = 8$ for both LBM and Fluent. Because of these results, at least $N = 8$ grid resolution is used for accuracy of simulations in LBM and Fluent.

Table 2. Number lattice units / finite volumes and CD predictions for steady-state flow (symmetry) with four grid resolutions (Re = 100)

	Number of lattice units/finite volumes	LBM (C_D)	Fluent (C_D)
$N = 4$	2620	6.26	6.46
$N = 8$	10480	5.96	6.72
$N = 12$	23868	5.95	6.74
$N = 16$	41536	5.96	6.74

Predictions are performed for Re = 160, 270, 530, 800, and 1070. In these computations, performed for the full channel domain (without symmetry plane, fig. 1), it is observed that the flow converges to a steady-state solu-

tion for Re = 160 and 270. An unsteady behavior with vortex shedding is observed for higher Re (Re = 530, 800, 1070). However, also for those Reynolds number, steady-state solutions are artificially obtained by employing symmetry (fig. 1), for better demonstrating the consequences of this assumption. In all unsteady computations, the time step size applied can be considered to be fairly small, which resulted in a resolution of a period in at least 1000 time steps and, in cell Courant numbers (*Co*) about 0.2 (based on bulk inlet velocity). For all full channel domain simulations, number of lattice units/finite volumes for the half height of the triangular cross-section is taken as N = 25. This grid resolution is enough for accuracy according to steady-state flow (symmetry) grid numbers study (tab. 2). Figure 6 displays, in the near-field of the TP, the unsteady/instantaneous streamlines, the unsteady/time-averaged streamlines, and the steady-state streamlines, as predicted by LBM for Re = 1070 (the steady-state solution shown in fig. 6(c) is enforced by solving the equations in the half-domain, applying the symmetry boundary condition of fig. 1. Results are displayed for full-domain, for post-processing purposes, by mirroring the solution around the symmetry plane in fig. 6(c). The instantaneous streamlines indicate the unsteady, and at any time non-symmetric flow structure behind the prism due to vortex shedding, fig. 6(a). The time-averaged streamlines appear symmetric around the channel mid-plane, of course, and exhibit a rather small re-circulation zone behind the prism, fig. 6(b). If the flow unsteadiness is neglected and a steady-state flow is enforced by artificially suppressing the unsteadiness by a symmetry plane, the size of the re-circulation zone is highly over-predicted, fig. 6(c). Additionally, when the symmetry is imposed to the flow, the vortex shedding instability eliminates and the length of the re-circulation zone increases linearly with respect to Reynolds number.

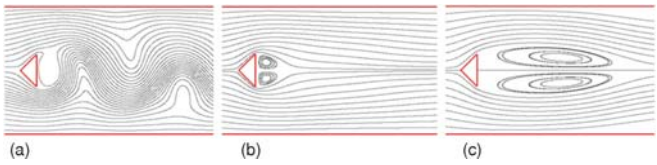

Figure 6. Streamlines predicted by LBM for Re = 1070; (a) unsteady/instantaneous, (b) unsteady/time averaged, (c) steady-state using symmetry plane

Figure 7 shows the comparison of the dimensionless skin friction (*C*) values of LBM and Abbasi *et al.* [7] at the channel bottom wall for Re = 160. One can observe that, dimensionless skin friction predictions of LBM and Abbasi *et al.* [7] are close with each other.

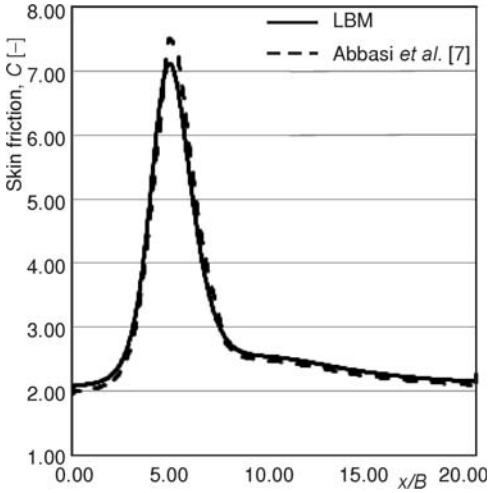

Figure 7. Skin friction values at the channel bottom wall for Re = 160

Table 3 compares the drag coefficient (time-averaged) and Strouhal number predicted by LBM and Fluent, for the unsteady flow at Re = 1070. Here, the frequency associated with the lift force on the prism is considered in determining the Strouhal number. A quite good agreement between the LBM and Fluent predictions are observed (tab. 3).

Table 3. C_D and St predicted for Re = 1070

	LBM	Fluent
C_D	6.40	6.46
St	0.35	0.34

Isotherms predicted by LBM for cases with and without triangular prism, using different modeling approaches are displayed in fig. 8, for Re = 1070. The unsteady-periodic pattern of the temperature field can be seen in fig. 8(a). This simulation is confined case, because channel flow with built-in triangular prism is setup with wall boundary conditions. This isotherms clearly shows that, the von Karman vortices in the wake are inverted with respect to the classical configuration in the unconfined case (channel flow with symmetry conditions) in fig. 8(a) [25]. One can observe that the temperature field of the (artificially obtained) steady-state solution, fig. 8(c) does not differ much from that of the solution without prism, fig. 8(d) except in the near-field of the prism, without necessarily implying a remarkable heat transfer enhancement.

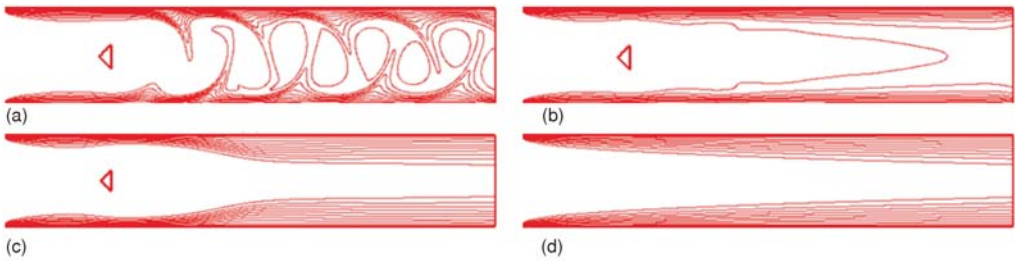

Figure 8. Isotherms predicted by LBM for Re = 1070; (a) unsteady/instantaneous with TP, (b) unsteady/time averaged with TP, (c) steady-state with TP, (d) steady-state, without TP

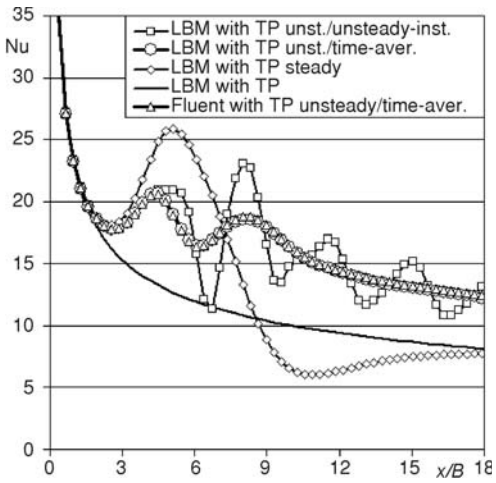

Figure 9. Predicted Nu along channel wall (Re = 1070)

The time-averaged results of the unsteady solution, fig. 8(b), differ from the steady-state solution, (fig. 8c), and imply a more substantial heat transfer enhancement. Predicted Nasselt number variations along channel wall for Re = 1070 are shown in fig. 9. Results neglecting flow unsteadiness (using an artificial symmetry plane) show an increase of the Nasselt number in the near-field of TP, purely due to blockage effects. However, behind TP, steady-state Nasselt number predictions undershoot the values of the case without TP (deceleration behind TP). A higher mean Nasselt number is still predicted. However, this artificially obtained steady-state result does not have much physical significance. The variations of the instantaneous and the time-averaged Nasselt number are also displayed in fig. 9. The time-averaged Nasselt number shows a local peak nearly at the same location as the stationary solution, which is, but, slightly lower. This is followed by a secondary local peak in downstream. It is interesting to see that the time- averaged Nasselt number values are much higher than those of the case without prism and those of the stationary computation with TP, especially in the downstream region. Thus, one can see that the heat transfer to channel walls can be enhanced by a triangular prism, and this effect is mainly due to the unsteady-periodic vortex shedding. Again, a perfect agreement of the LBM predictions with those of Fluent is observed.

ISLBM results

Figure 10 shows the non-uniform grid used for ISLBM and Fluent computations, for Re = 530. This grid resulted from a grid-independency study performed by Fluent and, thus, represents an optimal grid for a finite volume based CFD calculation. Thus, a performance comparison of based on this grid can be seen to be a fair one. Figure 11 compares profiles of the time-averaged axial velocity along traversal direction, at an axial position half triangle base behind TP, predicted by ISLBM (CSOI, USOI) and Fluent, for Re = 530. All predictions show a quite good agreement.

Figure 10. Grid for ISLBM study (Re = 530)

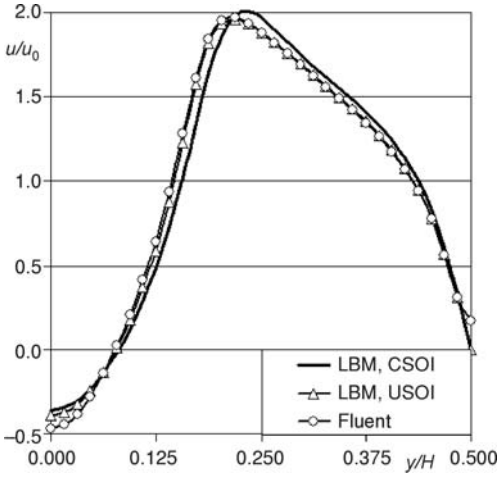

Figure 11. Axial velocity along transversal direction at an axial distance of *B*/2 downstream the prism (Re = 530)

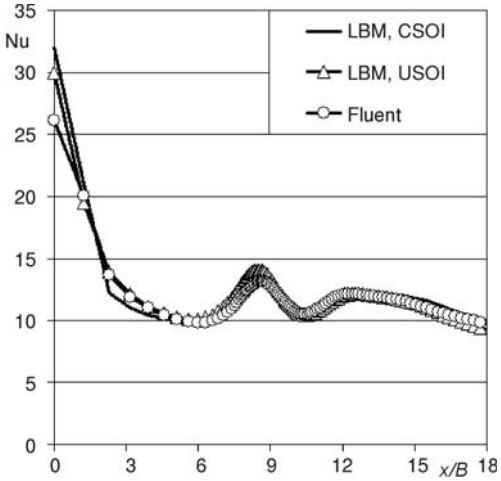

Figure 12. Predicted Nasselt number along channel wall (Re = 530)

Time-averaged Nu variations along channel wall predicted for Re = 530 by ISLBM (CSOU, USOI) and Fluent are shown in fig. 12. Again, a quite close agreement of the predictions can be observed.

Table 4 presents computing times required for one period, for the unsteady/periodic computation, for Re = 530. One can see that LBM requires much smaller computer times.

Table 4. Unsteady computing times for one period (Re = 530)

	LBM	Fluent
User time [s]	27	703

Conclusions

The Lattice Boltzmann Method (LBM) is used to computationally investigate the laminar forced convection in a 2-D channel with a built-in triangular prism, assuming incompressible flow with constant material properties. Both the traditional LBM, and the interpolation supported LBM techniques are implemented. Predictions show that the presence of a triangular prism affects the flow and heat transfer patterns for the steady-state (Re < 300) and unsteady/pe-

riodic flow (Re > 300) regimes. It is observed that heat transfer can be enhanced by the presence of a triangular prism, especially for the high Reynolds numbers, where an unsteady-periodic flow structure (vortex shedding) is observed, which appears to be the main mechanism responsible for this enhancement. It is also demonstrated that an artificial suppression of flow unsteadiness (*e. g*. by a symmetry plane) can lead to large errors in the prediction of the time-averaged values. The developed LBM code is validated by means of comparisons with a well-established commercial CFD code. It is also shown that computing times required by LBM are much smaller compared to the finite volume methods, especially for unsteady problems.

Nomenclature

A – projected prism area, [m^2]
a – thermal diffusivity (= $k/\rho c_p$), [m^{2}s^{-1}]
B – base of triangular prism cross-section
C – skin friction [= $2(\partial(u/u_0)/\partial y)$], [–]
c – lattice speed, [ms^{-1}]
C_D – drag coefficient [= $F_D/(0.5ru_0^2A)$]
c_p – isobaric specific heat capacity, [JK^{-1}]
c_s – lattice sound speed, [ms^{-1}]
Co – cell courant no. based on u_0(= $u_0\delta t/\delta$), [–]
D_h – hydraulic diameter (= $2H$), [m]
$\vec{e}_\alpha$ – discrete lattice velocity set, [ms^{-1}]
F_D – drag force, [Nm^{-2}]
f – dominant frequency, [1s^{-1}]
f_α – discrete density distribution function, [kgm^{-3}]
g_α – discrete temperature distribution function, [K]
H – channel height (= 4 B), [m]
h – heat transfer coefficient [= $q/(T_W - T_{F,0})$, [Wm^{-2}K^{-1}]
k – thermal conductivity, [WmK^{-1}]
LI – linear interpolation
Nu – Nusselt number (= hD_h/k)
p_0 – reference static pressure, [Pa]
Pr – Prandtl number (= $\mu c_p/k$)
q – heat flux, [Wm^{-2}]
Re – Reynolds number (= $\rho u_0 D_h/\mu$), [–]
St – Strouhal number (= fB/u_0)
T – temperature, [K]
t – time, [s]
u – axial velocity, [ms^{-1}]
u_0 – mean inlet velocity, [ms^{-1}]
$\vec{x}$ – position vector
x,y – 2-D Cartesian co-ordinates

Greek symbols

δ – lattice unit (distance between two neighboring lattice nodes) [m]
δ_t – time step, [s]
θ – dimensionless temperature [= $(T - T_{F,0})/(T_W - T_{F,0})$]
μ – dynamic viscosity, [kgms^{-1}]
ν – kinematic viscosity, [m^{2}s^{-1}]
ρ – density, [kgm^{-3}]
ρ_0 – reference density, [kgm^{-3}]
ω – collision frequency for momentum transfer, [1s^{-1}]
ω_T – collision frequency for energy transfer, [1s^{-1}]

Acronims

CSOI – central second order interpolation
TP – triangular prism
USOI – upwind second order interpolation

Sub- and superscripts

F – fluid
eq – equilibrium value
W – wall
0 – Inlet
~ – post-collision state

References

[1] Wesfreid, J. E., *et al*., Global Mode Behavior of the Streamwise Velocity in Wakes, *Journal de Physique (France), 6* (1996), 10, pp. 1343-1357
[2] Bosch, G., *et al*., Experiments on the Flow Past a Square Cylinder Placed Near a Wall, *Exp. Thermal Fluid Sci. 13* (1996), 3, pp. 292-305
[3] Nakagawa, S., *et al*., Heat Transfer in Channel Flow Around a Rectangular Cylinder, *Heat Transfer-Japanese Reseach, 27* (1998), 1, pp. 84-94
[4] Biswas, G., *et al*., Numerical Investigation of Mixed Convection Heat Transfer in a Horizontal Channel with a Built-in Square Cylinder, *Num Heat Transfer Part A, 18* (1990), 2, pp. 173-188

[5] Valencia, A., Cid, M., Turbulent Unsteady Flow and Heat Transfer in Channels with Periodically Mounted Square Bars, *Int. J. Heat Mass Transfer, 45* (2002), 8, pp. 1661-1673
[6] Gupta, M., *et al*., Flow Structure and Heat Transfer Analysis in a Laminar Channel Flow with Built-in Side-by-Side Dual Triangular Prism, *Journal of Engineering and Technology, 1* (2011), 2, pp. 65-69
[7] Abbasi, H., *et al*., Numerical Investigation of Forced Convection in a Horizontal Channel with a Built-in Triangular Prism, *Journal Heat Transfer, 124* (2002), 3, pp. 571-573
[8] Chattopadhyay, H., Augmentation of Heat Transfer in a Channel Using a Triangular Prism, *Int J Thermal Sciences, 46* (2007), 5, pp. 501-505
[9] Ellahi, R., *Steady and Unsteady Flow for Newtonian and Non-Newtonian Fluids: Basics, Concepts and Methods*, VDM Publishing GmbH & Co. KG, Germany, 2009
[10] Mohammad, A. A., *Applied Lattice Boltzmann Method*, SURE Print, Dalbrent, Canada, 2007
[11] Succi, S., *The Lattice Boltzmann Equation for Fluid Dynamics and Beyond*, Clarendon, Oxford, UK, 2001
[12] Benim, A. C., *et al*., Application of the Lattice Boltzmann Method to Steady Incompressible Laminar Hgh Re Flows. *Proceedings*, 7th IASME/WSEAS International Conference Fluid Mechanics and Aerodynamics, Moscow, 2009, pp. 220-225
[13] ***, *Fluent 6.3, User's Guide*, Fluent Inc, Lebanon, 2009
[14] Moussaoui, M. A., *et al*., Prediction of Heat Transfer in a Plane Channel Built-in Three Heated Square Obstacles Using an MRT Lattice Boltzmann Method, *Proceedings*, 6th International Conference on Computational Heat and Mass Transfer, Guangzhou, China, 2009, pp. 176-181
[15] He, X., *et al*., Some Progress in Lattice Boltzmann Method. Part I. Nonuniform Mesh Grids, *Journal of Computational Physics, 129* (1996), 2, pp. 357-363
[16] He, X., Doolen, G., Lattice Boltzmann Method on Curvilinear Coordinates System: Flow Around a Circular Cylinder, *Journal of Computational Physics, 134* (1997), 2, pp. 306-315
[17] He, X., *et al*., Some Progress in the Lattice Boltzmann Method: Reynolds Number Enhancement in Simulations, *Physica A., 239* (1997), 1-3, pp. 276-285
[18] Lu, Z., *et al*., Large Eddy Simulations of a Stirred Tank Using the Lattice Boltzmann Method on a Nonuniform Grid, *J. Computational Physics, 181* (2002), 2, pp. 675-704
[19] Niu, X. D., *et al*., Investigation of Stability and Hydrodynamics of Different Lattice Boltzmann Methods, *J. Statistical Physics, 117* (2004), 3, pp. 665-679
[20] Sunder, C. S., *et al*., A Detailed Performance Analysis of the Interpolation Supplemented Lattice Boltzmann Method on the Cray T3E and Cray X1, *The International Journal of High Performance Computing Applications, 20* (2006), 4, pp. 557-570
[21] Bhatnagar, P., *et al*., A Model for Collisional Processes in Gases I: Small Amplitude Processes in Charged and Neutral One-Component System, *Phys Review, 94* (1954), 3, pp. 511-525
[22] He, X., Luo, L. S., Lattice Boltzmann Model for the Incompressible Navier-Stokes Equation, *Journal Statistical Physics, 88* (1997), 3-4, pp. 927-944
[23] Sukop, M. C., Daniel, T. T. Jr., *Lattice Boltzmann Modelling – An Introduction for Geoscientist and Engineers*, Springer, Berlin, 2006
[24] Bejan, A., *Heat Transfer*, John Wiley & Sons Inc., New York, USA, 1993
[25] Camarri, S., Giannetti, F., On the Inversion of the von Karman Street in the Wake of a Confined Square Cylinder, *J. Fluid Mech., 574* (2007), March, pp. 169-178

Paper submitted: January 5, 2012
Paper revised: May 22, 2012
Paper accepted: July 10, 2012